CHALMERS

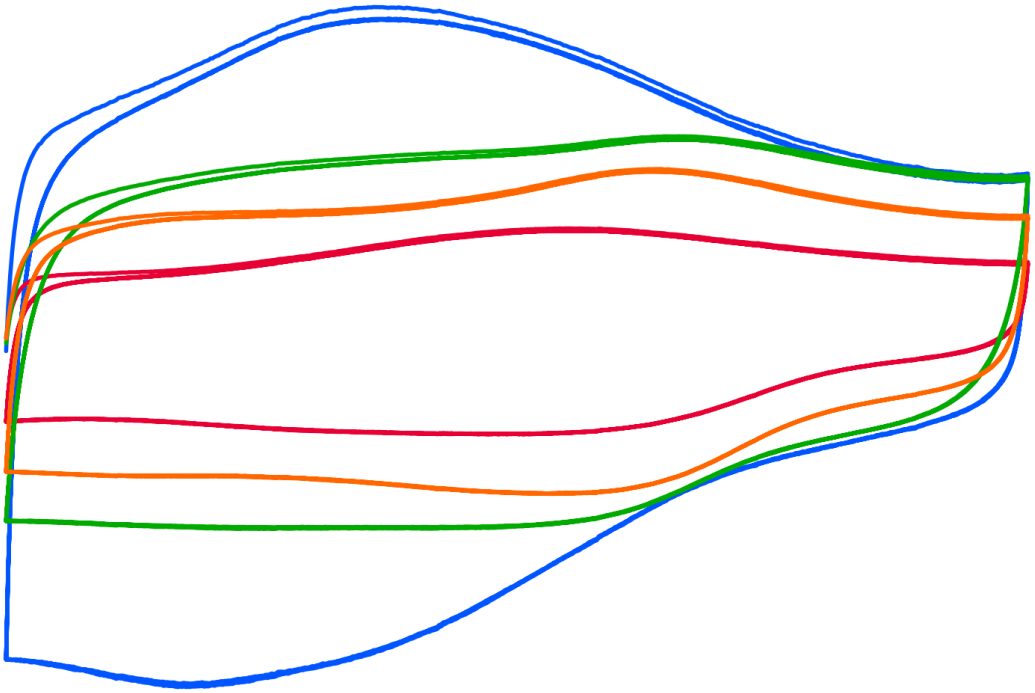

Aqueous Supercapacitors Based on Polymer-Biomass Composites

A Comparative Performance Analysis of PEDOT:F, PEDOT:PSS, and PBFDO with Sodium Lignosulfanate Additive

Bachelors's thesis in Chemical Engineering

YOHAN ZALEM

DEPARTMENT OF CHEMICAL ENGINEERING

CHALMERS UNIVERSITY OF TECHNOLOGY
Gothenburg, Sweden 2026
www.chalmers.se

Bachelor's thesis 2026

Aqueous Supercapacitors Based on Polymer-Biomass Composites

A Comparative Performance Analysis of PEDOT:F, PEDOT:PSS, and PBFDO with Sodium Lignosulfonate Additive

YOHAN ZALEM

CHALMERS

Department of Chemical Engineering
Division of Applied Chemistry
Chalmers University of Technology
Gothenburg, Sweden 2026

Aqueous Supercapacitors Based on Polymer-Biomass Composites: A Comparative Performance Analysis of PEDOT:F, PEDOT:PSS, and PBFDO with Sodium Lignosulfonate Additive
YOHAN ZALEM

Supervisor: Mathis Brette Mortensen, Department of Applied Chemistry
Examiner: Ergang Wang, Department of Applied Chemistry

Bachelors's Thesis 2026
Chemical Engineering
Division of Applied Chemistry
Chalmers University of Technology
SE-412 96 Gothenburg
Telephone +46 31 772 1000

Cover: Graph showing the CV measurment of PBFDO and PBFDO in different lignsosulfonate compositions at 100 mV/s

Typeset in LaTeX
Printed by Chalmers Reproservice
Gothenburg, Sweden 2026

Aqueous Supercapacitors Based on Polymer-Biomass Composites: A Comparative Performance Analysis of PEDOT:F, PEDOT:PSS, and PBFDO with Lignosulfanate Additive

Department of Some Subject or Technology
Chalmers University of Technology

Abstract

The development of sustainable aqueous supercapacitors requires the integration of high-performance conductive materials and abundant, environmentally friendly resources. This thesis investigates the electrochemical performance of composite electrodes comprising of conjugated polymers and lignosulfonate, a low-cost biomass derivative theoretically capable of providing additive pseudocapacitance through quinone-based reversible redox reactions. A comprehensive comparative analysis was conducted between established p-type polymers (PEDOT:F and PEDOT:PSS) and a novel, ultra-highly conductive n-type polymer, poly(benzodifurandione) (PBFDO). The active materials were deposited onto plasma-treated carbon paper substrates via a controlled sequential drop-casting method and evaluated in symmetrical two-electrode Swagelok cells utilizing an aqueous perchloric acid electrolyte.

Baseline electrochemical characterization via Cyclic Voltammetry (CV), Galvanostatic Charge-Discharge (GCD), and Electrochemical Impedance Spectroscopy (EIS) revealed that pristine PBFDO vastly outperformed both PEDOT derivatives. Evaluated at a low comparative current density of 0.25 A/g, PBFDO exhibited superior specific capacitance, exceptional structural resilience, and minimal Equivalent Series Resistance (ESR).

Contrary to the central hypothesis, the incorporation of unmodified lignosulfonate severely degraded the performance of all tested polymers. Rather than acting as a synergistic redox contributor, the water-soluble and electrically insulating lignosulfonate acted as an electrochemically inactive dead weight. While the p-type PEDOT composites suffered catastrophic electrochemical failure at a 1:1 polymer-to-lignin mass ratio, the self-doped n-type PBFDO matrix demonstrated remarkable structural resilience. Although the specific capacitance of PBFDO systematically declined as the lignin concentration increased across 3:1, 1:1, and 1:3 mass ratios, it maintained its fundamental charge-storage mechanisms without the massive internal resistance spikes observed in the p-type cells. Ultimately, while highlighting the limitations of physically blending raw lignosulfonate in aqueous electrolytes, this study unequivocally establishes the novel n-type PBFDO network as a premier, highly robust conjugated polymer for next-generation energy storage applications.

Keywords: Aqueous Supercapacitors, Conjugated Polymers, PBFDO, PEDOT, Lignosulfonate, Polymer-Biomass Composites, n-Type Polymers, Pseudocapacitance, Electrochemical Characterization, Energy Storage.

Acknowledgements

I would like to express my sincere gratitude to my supervisor, Mathis Brette Mortensen, for their invaluable guidance, insightful feedback, and continuous support throughout the course of this bachelor thesis. Their patience, insightful feedback, and encouragement have been instrumental in helping me navigate the complexities of this project and bringing this work to fruition
I am also deeply grateful to my examiner, Ergang Wang, for their invaluable assistance in setting up the foundation for this project, sharing their insightful knowledge, and taking the time to evaluate my work.
A special thanks goes to Jianzhou Li for their practical assistance and collaboration throughout the lab work. Their support and shared experience made the research process significantly smoother and more enjoyable.
Finally, thank you to my family and friends for their unwavering encouragement during my studies.

Yohan Zalem, Gothenburg, June 2026

List of Acronyms

Below is the list of acronyms that have been used throughout this thesis listed in alphabetical order:

AC	Alternating Current
CV	Cyclic Voltammetry
EDLC	Electrical Double-Layer Capacitance
EIS	Electrochemical Impedence Spectroscopy
ESR	Equivalent Series Resistance
GCD	Galvanostatic Charge-Discharge
LUMO	Lowest Unoccupied Molecular Orbital
OFGs	Oxygen Functional Groups
PBFDO	Poly(benzodifurandione)
PEDOT	Poly(3,4-ethylenedioxythiophene)
PEDOT:F	Poly(3,4-ethylenedioxythiophene) fluorinated derivative
PEDOT:PSS	Poly(3,4-ethylenedioxythiophene):polystyrene sulfonate

Nomenclature

Below is the nomenclature of indices, sets, parameters, and variables that have been used throughout this thesis.

Nomenclature

Variables and Mathematical Parameters

C_{sp}	Specific capacitance of a single electrode
C	Measured absolute capacitance of the entire two-electrode cell
C_{cell}	Total capacitance of the symmetrical cell
C_1, C_2	Capacitance of electrode 1 and electrode 2, respectively
m_{tot}	Combined total mass of the active material on both electrodes
m_{single}	Mass of the active material on a single electrode
I	Applied current
$\mathrm{d}V/\mathrm{d}t$	Slope of the Galvanostatic Charge-Discharge (GCD) curve over time
e^-	Electron
H^+	Proton

Units of Measurement

F g^{-1}	Farads per gram (Specific capacitance)
S cm^{-1}	Siemens per centimeter (Electrical conductivity)
eV	Electron-volts (Energy level)
μL	Microliters (Volume)
mg	Milligrams (Mass)
mm	Millimeters (Distance/Diameter)
°C	Degrees Celsius (Temperature)

Contents

List of Figures

1
Introduction

1.1 The Demand for Advanced Energy Storage

The rapid depletion of global fossil fuel resources along with the rising severity of environmental pollution and climate change, has led to a huge requirement for clean renewable energy sources as well as efficient electrical energy storage devices. As society transitions toward more sustainable energy sources, the need for efficient and reliable energy storage technologies becomes increasingly important [1, 2]. In this regard, supercapacitors, also known as electrochemical capacitors, have come to function as a bridge between conventional dielectric capacitors and rechargeable batteries due to their high potential to provide high power density along with high rates of charge/discharge cycles, despite their low energy density compared to batteries [3, 4]. To bridge this gap between energy density, current research is highly focused on developing new types of pseudocapacitive materials that can store energy through high-rate reversible Faradaic redox reactions [1, 2].

1.2 Conjugated Polymers and Biomass-Derived Materials

The electrochemical performance of supercapacitors is inherently related to their electrode materials' structural and chemical characteristics. Conjugated polymer materials have been widely studied for their potential use as supercapacitor electrode materials due to their high theoretical specific capacitance, tunable electrical characteristics, low cost, and minimal environmental impact [5, 6]. Among these, PEDOT:PSS derivatives have been widely studied as one of the best p-type mixed ion-electron conductor materials, ensuring electroactive performance in organic devices [7]. However, these materials have shown considerable degradation of their structural integrity during charge-discharge cycling. Furthermore, there is a scarcity of n-type conjugated polymers, which have historically shown lower electrical conductivity compared to their p-type counterparts.
Recently, a novel self-doped n-type conjugated polymer, poly(benzodifurandione) (PBFDO), was successfully synthesized using a cost-effective and scalable selenium dioxide (SeO_2)-catalyzed polymerization method. When the reaction is conducted for 48 hours using 0.1 equivalents of SeO_2, it achieves a high monomer conversion rate of 91%. Although the mixture forms a gel during the late stages of this process due to increased viscosity, which prevents complete conversion, the resulting

polymer exhibits unprecedented electrical conductivity exceeding 5000 10 S cm^{-1}. Furthermore, this catalytic method allows for straightforward purification using only centrifugation and filtration, bypassing the need for expensive and time-consuming dialysis [5, 8, 9].
To increase their energy storage capacity, these conjugated polymer materials could incorporate redox-active biomolecules as additives. A prime candidate for this is lignin, one of the most prevalent natural biopolymers occurring in nature with it being present in approximately 15-25 wt% in wood. Among these, lignosulfonate, a water-soluble form derived as a byproduct in the sulfite pulping process for wood pulp production, is a low-cost and renewable material. In energy storage devices, the quinone and hydroquinone groups in lignin have shown reversible electron and proton transfer capability which gives rise to large pseudocapacitive effects. Lignosulfonate can be combined with conducting polymer electrodes such as PEDOT and PBFDO. This enables the wiring and confinement of lignin in its insulating state, thus making full use of its potential for reversible redox reactions [2].

1.3 Substrate Engineering via Plasma Treatment

To examine such active materials, porous carbon paper is often used as an electrode current collector because its porosity allows for high active material loading and provides a unique interconnected network. However, there are certain drawbacks to carbon fiber material, such as an insufficient amount of oxygen-containing groups on the surface of the material and a high hydrophobic nature [10, 11]. This high hydrophobic nature is a major problem in uniformly casting an aqueous dispersion of polymers and lignin onto the electrodes.
Plasma treatment is an innovative and environmentally friendly solution to this problem. When a carbon material is subjected to plasma treatment, essential oxygen functional groups (OFGs) are introduced to the carbon structure, creating defects on the material's surface [12, 13]. This electrochemical activation improves the hydrophilicity of the carbon paper, allowing a more efficient infiltration of the electrolyte into the electrodes during cell operation[11, 13].

1.4 Scope and Objectives of the Thesis

The ultimate goal of this thesis is to construct, assemble, and analyze symmetrical supercapacitor cells of lignosulfonate combined with each conjugated polymer. We are interested in comparing a known p-type polymer (PEDOT and its derivatives such as PEDOT:F and PEDOT:PSS) with a novel n-type polymer, PBFDO.
The methodology that this thesis will be based upon will include utilizing a plasma-treated carbon paper substrate that will be used to optimize and ensure that a polymer-lignosulfonate blend is deposited uniformly by drop-casting. The electrodes will then be assembled into a symmetrical two-electrode cell design utilizing a glass fiber separator and aqueous perchloric acid as the electrolyte solution. While a three-electrode cell is commonly used in material characterization and testing, a two-electrode cell design is universally accepted as being the most accurate and reliable

method for determining and predicting a material's performance in a packaged real-world supercapacitor device [4].
The thesis investigates charge storage mechanisms of composites through detailed electrochemical experiments which include Cyclic Voltammetry (CV), Galvanostatic Charge-Discharge (GCD), and Electrochemical Impedance Spectroscopy (EIS). The research will identify which conjugated polymer combinations produce the strongest interactive effects with lignosulfonate while determining the lignin-to-polymer ratio which produces maximum specific capacitance and cycling stability in aqueous supercapacitors.

2

Theory

2.1 Principles of Aqueous Supercapacitors

Supercapacitors function as essential energy storage devices which establish an energy storage performance standard that exists between conventional dielectric capacitors and rechargeable batteries. The system provides rapid power delivery through its ability to charge and discharge quickly while maintaining operational performance for extended periods. Supercapacitor systems develop their charge storage functionality through two primary charge storage mechanisms which develop their operational capabilities. The Electrical Double-Layer Capacitance (EDLC) system stores electrical charge through electrostatic storage at the boundary between the electrode and electrolyte interface. The use of materials with high specific surface areas which include activated carbon and carbon nanotubes enables the maximum accumulation of electrolyte ions. Pseudocapacitance systems store charge electrochemically through highly reversible, surface or near-surface Faradaic redox reactions. This mechanism enables solvated electrolyte ions to engage with electrode materials which include transition metal oxides and conjugated polymers to produce an energy density that exceeds EDLC systems [1].

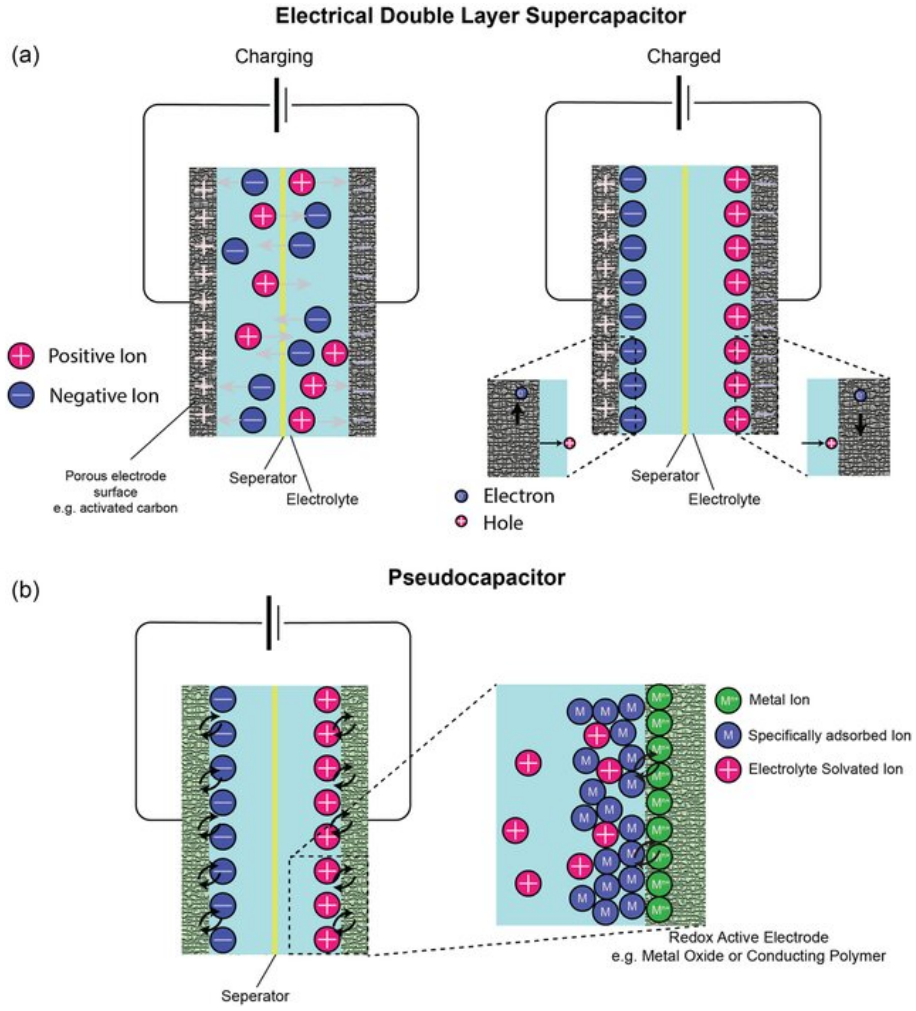

Figure 2.1: Schematic representation of storage mechanisms for a) EDLC and b) Pseudocapacitors[14].

2.2 Conjugated Polymers in Energy Storage

As pseudocapacitive electrode materials, conjugated polymers have become very desirable due to their tunable electrical conductivity, low environmental impact, affordability, and flexibility [6, 15]. The conjugated polymers consists of a chain of alternately single and double bonds which provide delocalized π-electrons for efficient electron transport [6]. In the charge/discharge process, these polymers are doped and dedoped reversibly, that the counterions from electrolyte move into and out of the polymer backbone [1, 15].

Among p-type polymers, PEDOT:PSS and PEDOT:F, PEDOT (poly(3,4-ethylenedioxythiophene)) derivatives are the most successful p-type conjugated polymers because of their wide potential window, good stability, and high conductivity [1]. PEDOT:PSS is the most common form due to its water-dispersible property and good film-forming performance [16]. Whereas p-type conjugated polymers have been well developed, few n-type (electron-conducting) polymers, such as poly(benzimidazobenzophenanthroline) (BBL), were studied and applied for en-

ergy storage applications [17]. PBFDO is a newly synthesized self-doped n-type conjugated polymer. Its electrical conductivity reaches up to approximately 5500 S cm^{-1}, which is unprecedented among the n-doped conjugated polymers, with an exceptionally low-lying Lowest Unoccupied Molecular Orbital (LUMO) level (near -5.18 eV) [5, 18]. Because of this low LUMO level, the PBFDO shows remarkable stability in oxygen and water, therefore, can work with aqueous electrolytes efficiently. It has been shown that in supercapacitors, PBFDO possesses a high specific capacitance (such as 202 F/g) and excellent rate capability which is dominated by the surface mediated 1-electron reduction charging storage mechanism [17, 18].

2.3 Doping Mechanisms in p-type and n-type Conjugated Polymers

Unlike traditional inorganic semiconductors where doping involves the insertion of trace elemental impurities into a crystal lattice, the "doping" of conjugated polymers is a reversible electrochemical redox process. In their pristine state, conjugated polymers behave as insulators or semiconductors with a moderate energy bandgap. However, through electrochemical oxidation or reduction, electrons are respectively extracted from or injected into the polymer backbone [6]. To maintain overall charge neutrality during this process, counterions from the surrounding electrolyte are inserted into or expelled from the semiconducting polymer matrix[1, 15].
This injection or extraction of electrons disrupts the alternating single and double bonds of the conjugated backbone, inducing a localized structural deformation—often transitioning from a benzoid to a quinoid geometric structure. These structural deformations create highly mobile, delocalized charge carriers known as polarons (a radical ion carrying a single charge) and bipolarons (a spinless ion carrying a double charge) [15, 18]. The movement of these polarons and bipolarons along and between the polymer chains is what transforms the material into a highly conductive, metallic-like state [3, 6].

2.3.1 p-Type Conjugated Polymers

p-Type Conjugated Polymers (PEDOT Derivatives) p-type (hole-doping) occurs when the polymer is electrochemically oxidized. During this process, electrons are removed from the polymer's Highest Occupied Molecular Orbital (HOMO), leaving behind positive charges (holes) on the backbone [6, 15]. To balance these positive charges, anions from the electrolyte must intercalate into the polymer film, or pre-existing cations must be expelled.
In the case of PEDOT:PSS, the polymer exists as a polyelectrolyte complex where the poly(styrene sulfonate) (PSS) acts not only as a water-dispersible template but also as a large, relatively immobile macromolecular counterion. However, because PSS is intrinsically insulating, its presence in the resulting solid film acts as a performance bottleneck that limits overall electronic conductivity The negatively charged sulfonate groups of PSS balance the positively charged, p-doped PEDOT chains. When a PEDOT:PSS electrode is operated in a supercapacitor during a forward

(charging) voltage sweep, additional positive holes are injected into the PEDOT backbone. To maintain electroneutrality, mobile positive cations are expelled from the PEDOT:PSS matrix into the electrolyte. During the reverse (discharging) sweep, the hole density in the polymer decreases, and cations from the electrolyte migrate back into the polymer film [1].

2.3.2 n-Type Conjugated Polymers

n-Type Conjugated Polymers relies on the electrochemical reduction of the polymer. Electrons are injected from the external circuit into the polymer's Lowest Unoccupied Molecular Orbital (LUMO), generating negatively charged polarons and bipolarons. Consequently, positive cations from the electrolyte must insert themselves into the polymer matrix to neutralize the negative backbone [6, 15].
Historically, developing stable n-type conjugated polymers for energy storage has been highly challenging [3]. Most conventional n-type polymers possess relatively high LUMO energy levels, making their negatively charged states highly reactive and vulnerable to oxidative degradation by ambient oxygen and water [19]. This ambient instability typically restricts their use in aqueous electrolytes. However, the novel n-type polymer poly(benzodifurandione) (PBFDO) circumvents these issues. PBFDO features a uniquely low-lying LUMO level of approximately -5.1 eV, which is sufficiently deep to make the polymer thermodynamically and kinetically stable against oxygen and water reduction reactions [19]. This allows PBFDO to operate efficiently and stably even in aqueous acidic media.
Furthermore, PBFDO is characterized by a groundbreaking self-doping mechanism. Rather than requiring complex external post-doping treatments, PBFDO achieves an in-situ reductive n-doping simultaneously during its oxidative polymerization synthesis. This creates an extraordinarily high intrinsic charge carrier density (up to 0.86 charges per repeating unit), yielding a metallic coherent charge transport and a breakthrough electrical conductivity of up to 2000 S/cm without the need for insulating side chains [9].
During supercapacitor operation in an acidic electrolyte, PBFDO stores charge through a unique surface-mediated proton-coupled mechanism. Upon charging (n-doping), electrons are injected into the PBFDO backbone. Simultaneously, protons (H^+) that were bound to the polymer's carbonyl groups deintercalate and are expelled into the acidic electrolyte to balance the incoming negative electrons, forming negative polarons. Upon discharging, the process reverses: protons from the electrolyte re-intercalate and bond to the PBFDO main chain, neutralizing the negative charge as electrons are released back through the external circuit [5]. This rapid exchange of protons facilitates exceptionally fast kinetics, contributing to the high specific capacitance and power density of the material [5].

2.4 Lignosulfonate as a Redox-Active Biomolecule

Lignin is Earth's second most abundant biopolymer behind cellulose and constitutes the major structural constituent of wood. Lignosulfonate, a water-soluble technical lignin produced as a byproduct in sulfite pulping, is a sustainable and inexpensive

material for energy storage. The electrochemical activity of lignin is derived from the abundant quinone/hydroquinone substructures present within the lignin backbone. These functional groups are capable of undergoing readily reversible Faradaic reactions, the consumption and release of electrons and protons ($2e^-/2H^+$) throughout the discharge and charge processes. With the use of perchloric acid for this process the abundance of protons (H^+) in the aqueous electrolyte will be more than adequate to facilitate this redox behavior. Despite its inherent potential, two primary problems exist for utilizing lignin: its electrically insulating nature and the solubility of lignosulfonate in aqueous electrolytes which typically results in prompt self-discharge and extensive capacity fade. These two limitations can be overcome by electrically wiring and structurally confining lignin [2]. By mixing the lignosulfonate with conjugated polymers such as PEDOT:PSS, PEDOT:F and PBFDO, the conductive polymers act as both a physical scaffold and a three-dimensional current collector to prohibit dissolution of lignin in the electrolyte and provide sufficient electrically connectivity for the quinone functional groups to act as a highly electrochemically active pseudocapacitive material [2, 15].

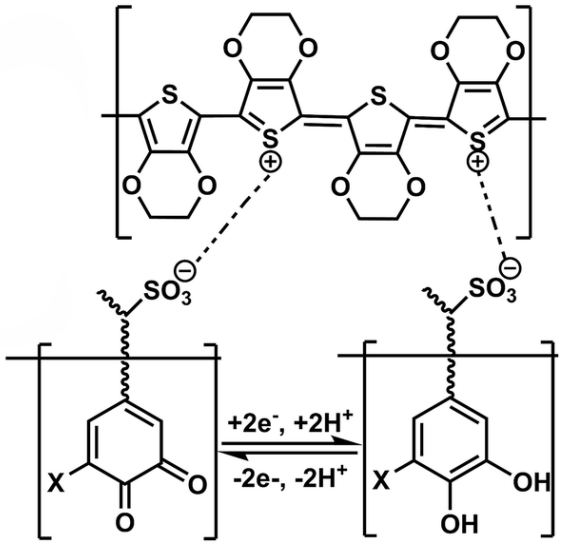

Figure 2.2: Schematic of the reversible ortho-quinone/hydroquinone redox mechanism, $2e^-/2H^+$, occurring on the lignosulfonate backbone. Adapted from [20].

2.5 Electrochemical Characterization Techniques

In order to ascertain the actual performance of the synthesized composite materials, a 2-electrode symmetrical Swagelok cell is employed. 3-electrode beaker cells are used to individually study the electrochemical behavior of a single material, while a symmetrical 2-electrode Swagelok cell represents a more accurate representation of how the material will perform in a packaged, commercial supercapacitor device [4, 17]. All electrochemical tests are performed using the following three methods:

Cyclic Voltammetry (CV): The CV test detects how current changes when voltage increases at a constant scan rate. While pure EDLCs exhibit symmetrical,

rectangular CV curves, pseudocapacitors, such as the polymer-lignin composites, show quasi-rectangular shapes with wide anodic and cathodic peaks because they contain reversible Faradaic redox reactions, which lead to the observed pseudocapacitor behaviour [1, 15].

Galvanostatic Charge-Discharge (GCD): GCD measures voltage vs time under a constant applied current. This method provides a direct measurement of the specific capacitance, energy density, and power density of the cell. Ideal capacitive behavior yields symmetrical, triangular curves, while any instantaneous voltage drop at the beginning of discharge (the IR drop) quantifies the equivalent series resistance (ESR) of the cell [1, 4].

Electrochemical Impedance Spectroscopy (EIS): The EIS test uses a small alternating current (AC) signal to evaluate the cell's impedance across various frequency ranges. The data is typically presented through Nyquist plots, which show imaginary impedance versus real impedance. The x-axis high-frequency intercept shows internal ohmic resistance. The size of the high-frequency semicircle represents charge transfer resistance at the electrode-electrolyte interface, and the low-frequency linear behavior (Warburg impedance) represents how effectively the ion is diffused through the porous structure of the electrode[2, 11, 21].

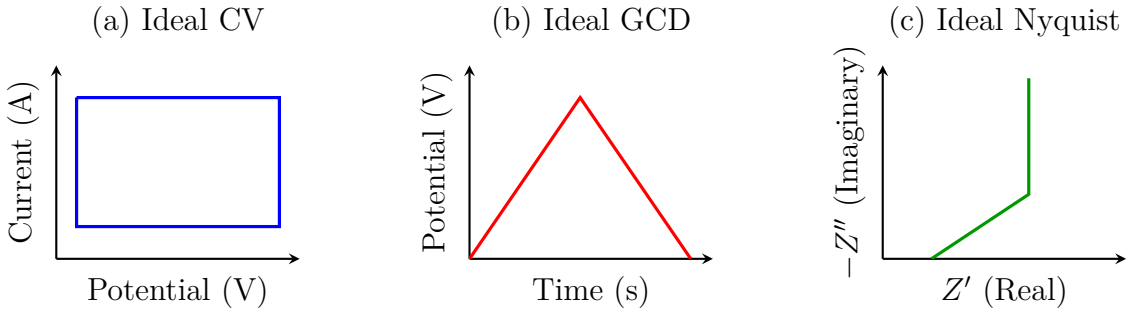

Figure 2.3: Theoretical ideal electrochemical behavior of an electric double-layer capacitor (EDLC) in a 2-electrode cell. Demonstrates its performance through three different tests which include (a) Cyclic Voltammetry that produces a rectangular output pattern which demonstrates fast current changes, (b) Galvanostatic Charge-Discharge test that produces a symmetrical triangular pattern which has no IR-drop, and (c) Nyquist plot which shows the equivalent series resistance (ESR) at the x-axis, followed by the 45° porous diffusion phase which follows the ideal 90° capacitive line.

3
Methods

3.1 Substrate Preparation and Surface Modification

For current collection, carbon paper was chosen due to its 3D interwoven structure combined with its great chemical stability. To prepare the substrates, plasma treated carbon paper was punched into circular discs with a diameter of 12 mm.

3.2 Fabrication of Polymer-Lignosulfonate Electrodes

The active electrode materials were prepared by mixing the selected conjugated polymers (PEDOT:F, PEDOT:PSS, and PBFDO) with lignosulfonate. Since the individual polymer dispersions used had different mass concentrations (w%) on their own, individualized lignosulfonate solutions with matching concentrations needed to be prepared for each particular polymer. Lignosulfonate was dissolved in dimethyl sulfoxide (DMSO) at matching percentage by weight to the percentage weight of the specific polymer that was going to be used [5, 16]. This step was important to ensure that the volume mixing will result in the correct weight ratios of solids in the final composite.
The specific lignin-to-polymer weight ratios were selected based on the type of polymer. PEDOT:F and PEDOT:PSS were synthesized and analyzed at the specific mass ratio of 1:1. For the newly synthesized n-type polymer PBFDO, a wider analysis range was applied and the lignin-to-PBFDO mass ratios of 1:1, 3:1 and 1:3 were chosen. The polymer dispersion and the correct matching lignosulfonate solution was mixed in a separate glass vial. In order to incorporate completely the polymer matrix and achieve homogeneous distribution of the active redox lignosulfonate component in the composite, the solutions were sonicated for 10 minutes at room temperature and as a result breaking up all possible aggregates to obtain a highly homogeneous mixture.
The homogeneous polymer-lignin dispersions were then deposited onto the plasma treated carbon paper substrate by successive drop casting. In order to obtain uniform layer on the hydrophilic carbon fiber the amount of dropped liquid had to be precisely 20 μL at a time. The electrodes were dried under vacuum at 50 °C for one hour to ensure slow evaporation of the solvent, and particularly the relatively high-boiling point DMSO, to successfully fuse the active material onto the

substrate. The drop-casting-drying process was repeated until the total mass of the active composite reached approximately 1 mg.

3.3 Symmetrical Swagelok Cell Assembly

In order to obtain realistic results regarding the composite electrodes' actual performance, they were integrated into a two-electrode symmetric Swagelok cell. Although three-electrode cells are typically used in fundamental materials characterization, they have a tendency to overestimate the measured capacitance due to their non-uniform voltage distribution and unbalanced counter electrode [4]. Hence, a symmetrical two-electrode system was chosen to most closely correspond to the physical arrangement, the internal voltages, and the charge transfer dynamics of a packaged commercial supercapacitor.
A pair of identical polymer-lignin coated carbon paper electrodes was mounted directly opposing one another within the Swagelok cell. A 13 mm diameter glass fiber separator was typically placed between the electrodes to prevent electronic short circuits while allowing efficient ion transport. For certain optimized configurations, three stacked separators were utilized. The two-electrode cell was activated by the addition of an optimized volume of 180 μL of an aqueous solution of perchloric acid to form the proton-rich electrolyte needed to accommodate the $2e^-/2H^+$ redox reaction of the lignosulfonate.

3.4 Electrochemical Characterization

All electrochemical measurements were performed on a Gamry Interface 1010B Potentiostat. The assembled Swagelok cells were characterized electrochemically by CV, GCD and EIS in order to thoroughly evaluate the energy storage capability.

3.5 Data Processing and Specific Capacitance Calculation

Custom Python scripts were created to automate the analysis of data produced by the Gamry potentiostat. These scripts read in the raw data and generated the CV, GCD and EIS (Nyquist) graphs. Additionally, Python scripts were written specifically to calculate the specific capacitance (C_{sp}) of active materials as measured via GCD testing. The specific capacitance of individual electrodes has been calculated according to such standardized methodologies for symmetrical two-electrode cell configurations.

$$C_{\text{sp}} = \frac{4 \times C}{m_{\text{tot}}} \tag{3.1}$$

In this equation:

- C is the measured absolute capacitance of the two-electrode cell calculated from the GCD discharge plot using $C = I/(dV/dt)$

- m_{tot} is the combined total mass of the active material on both electrodes.

The multiplier of 4 is necessary to adjust the cell capacitance and combined mass to represent the specific capacitance of a single electrode. In a symmetrical cell, the two electrodes act as two equivalent capacitors connected in series ($1/C_{\text{cell}} = 1/C_1 + 1/C_2$). Because the electrodes are close to identical ($C_1 = C_2$), the capacitance of a single electrode (C_1) is twice the measured cell capacitance ($2 \times C$). To express this per unit mass of a single electrode ($m_{\text{single}} = m_{\text{tot}}/2$), the calculation becomes $\frac{2 \times C}{m_{\text{tot}}/2}$, which simplifies to $\frac{4 \times C}{m_{\text{tot}}}$ [4]. This method ensures that the specific capacitance reported accurately reflects the performance of the polymer-lignin composite.

4

Results

4.1 Electrochemical Performance of Pristine Conjugated Polymers

To establish a baseline for comparative analysis, the pristine conjugated polymers, the p-type derivatives PEDOT:F and PEDOT:PSS, and the novel n-type poly(benzodifurandione), were first evaluated in symmetrical two-electrode Swagelok cells using an aqueous perchloric acid electrolyte.

Cyclic Voltammetry (CV) was performed across a range of scan rates (5 to 100 mV/s) to evaluate the charge storage mechanisms. The CV curves for all three pristine polymers (Figure 4.1b) exhibited the quasi-rectangular shapes featuring broad redox peaks that are characteristic of pseudocapacitive materials [15]. However, the current density responses varied drastically. PBFDO demonstrated exceptionally broad and symmetrical CV curves with a larger integrated area, corresponding to a significantly higher capacitance compared to both PEDOT:F and PEDOT:PSS. This indicates a highly reversible surface-mediated charge storage mechanism and superior ion accessibility within the PBFDO matrix.

Galvanostatic Charge-Discharge (GCD) measurements were conducted at various current densities to quantify the specific capacitance and evaluate the equivalent series resistance (ESR). The initial portion of a GCD discharge curve typically exhibits an instantaneous voltage drop (the IR drop), which correlates directly to the internal resistance of the cell [4]. The pristine PBFDO electrode exhibited highly symmetrical, triangular charge-discharge profiles with a minimal IR drop, indicating excellent conductivity and efficient charge propagation. In contrast, PEDOT:F displayed a skewed triangular GCD profile with a noticeably larger IR drop, signifying higher internal resistance.

By comparing the maximum energy storage capacities obtained at a low applied current density of 0.25 A/g (Figure 4.1a), the specific capacitance of pristine PBFDO reached a peak value of 158.2 F/g. Under these same prolonged discharge conditions, PEDOT:F exhibited a slightly higher maximum capacitance 33.0 F/g compared to PEDOT:PSS 28.8 F/g.

However, evaluating the materials across a broader range of current densities revealed the severe kinetic limitations of PEDOT:F. Because PEDOT:F possesses a significantly higher Equivalent Series Resistance (ESR), its capacitance faded rapidly as the current demand increased. At higher, more practical current densities, PEDOT:PSS consistently outperformed PEDOT:F, demonstrating superior rate capability and lower internal resistance. Most importantly, the novel n-type

PBFDO vastly outperformed both p-type derivatives across the entire tested spectrum. PBFDO not only delivered the highest absolute capacitance, but also maintained its structural and electrochemical efficiency at high current densities, unequivocally demonstrating the superior charge storage capability of its self-doped network.

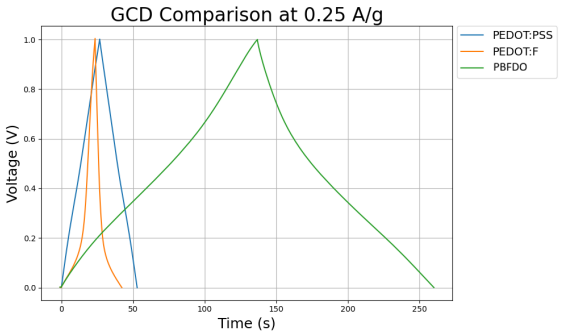

(a) GCD Comparison of PBFDO, PEDOT:F and PEDOT:PSS at 0.25 A/g

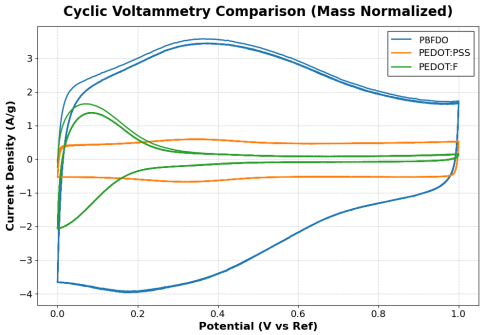

(b) CV comparison of PBFDO, PEDOT:F and PEDOT:PSS

Figure 4.1: GCD and CV comparison of the three conjugated polymers. (a) GCD curves at a current density of 0.25 A/g. (b) Mass-normalized CV curves. All electrochemical measurements were performed in a symmetrical two-electrode Swagelok cell configuration using an aqueous perchloric acid electrolyte.

4.2 Influence of Lignosulfonate on PEDOT-Based Supercapacitors

Following the baseline measurements, composite electrodes comprising lignosulfonate and the p-type conjugated polymers at a 1:1 mass ratio were evaluated. The underlying hypothesis was that the quinone/hydroquinone substructures within the lignin would undergo reversible $2e^-/2H^+$ faradaic reactions, thereby providing additive pseudocapacitance while being electrically wired by the conjugated polymer network.

However, the electrochemical data revealed that the incorporation of lignosulfonate severely impeded the performance of the p-type polymers. As observed in the CV plots for both PEDOT:F+Lignin and PEDOT:PSS+Lignin (1:1), the total integrated area under the curves collapsed significantly compared to their pristine counterparts. Specifically, the PEDOT:F+Lignin composite exhibited highly resistive, tilted CV curves with negligible current densities, indicating poor electron transfer and restricted ion diffusion.

The GCD measurements confirmed this severe degradation. The PEDOT:F+Lignin composite experienced a massive, near-instantaneous IR drop upon the initiation of discharge, resulting in an extremely short discharge time and a negligible specific capacitance. The PEDOT:PSS+Lignin composite fared marginally better but still suffered a reduction in capacitance compared to pure PEDOT:PSS. These results

suggest that the insulating nature of the lignosulfonate dominated the composite matrix, disrupting the percolation pathways of the PEDOT derivatives and blocking access to the electrochemically active sites.

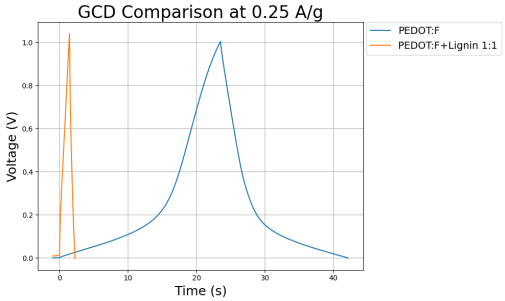

(a) GCD comparison of PEDOT:F and PEDOT:F+Lignin 1:1

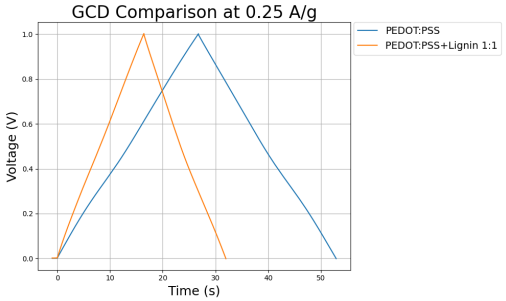

(b) GCD comparison of PEDOT:PSS and PEDOT:PSS+Lignin 1:1

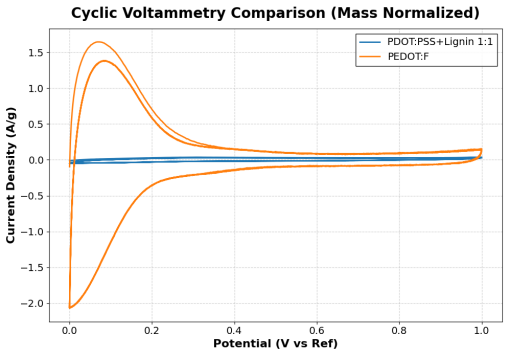

(c) CV comparison of PEDOT:F and PEDOT:F+Lignin 1:1

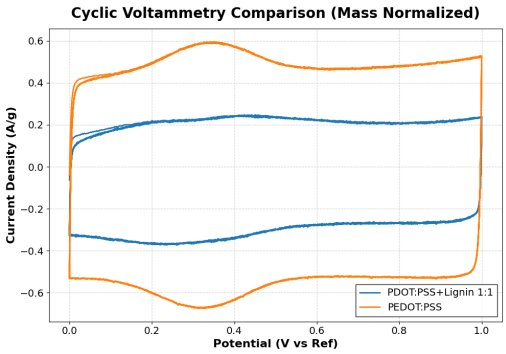

(d) CV comparison of PEDOT:PSS and PEDOT:PSS+Lignin 1:1

Figure 4.2: GCD and CV comparison of PEDOTF, PEDOT:F+Lignin 1:1, PEDOT:PSS and PEDOT:PSS+Lignin 1:1.

4.3 Optimization of PBFDO and Lignosulfonate Mass Ratios

Given the superior baseline performance of the n-type PBFDO polymer, a comprehensive ratio optimization study was conducted to determine if a specific polymer-to-biomass ratio could unlock the synergistic effects of the lignosulfonate. Composites were formulated and tested at PBFDO-to-Lignin ratios of 3:1, 1:1, and 1:3.
The mass-normalized CV comparison reveals a clear and systematic trend regarding the composite formulation. The pristine PBFDO electrode enclosed the largest CV area, directly corresponding to the highest charge storage capacity. The introduction of lignosulfonate resulted in a systematic decrease in the integrated CV area. The PBFDO+Lignin 3:1 composite (polymer-rich) retained a relatively large, quasi-rectangular CV profile, demonstrating the second-highest current density. As the

lignin content increased to 1:1 and subsequently to 1:3 (lignin-rich), the CV area progressively contracted.
Despite the overall contraction of the CV area with increasing lignin content, a distinct new anodic signal emerges at approximately +0.6 V vs Ref. This peak is attributed to the faradaic redox transition of surface-accessible quinone/hydroquinone moieties inherent to the lignosulfonate structure [22]. Interestingly, this localized molecular redox wave is more sharply pronounced than the faradaic signals of the pristine PBFDO. This occurs because PBFDO stores charge via broadly distributed energy states across its conjugated backbone, yielding a featureless pseudocapacitive envelope. In contrast, the quinone groups in lignin undergo localized, two-electron transfers at a specific thermodynamic potential, concentrating their current density into a discrete, distinct peak even as the bulk conductivity of the composite decreases [20].

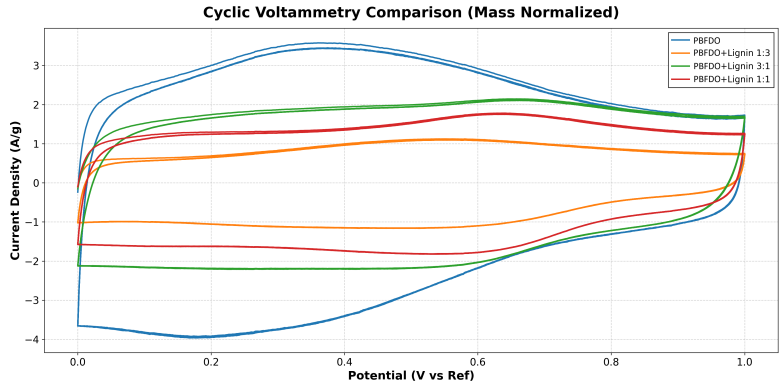

Figure 4.3: CV comparison of PBFDO and PBFDO with lignin blends in different mass ratios.

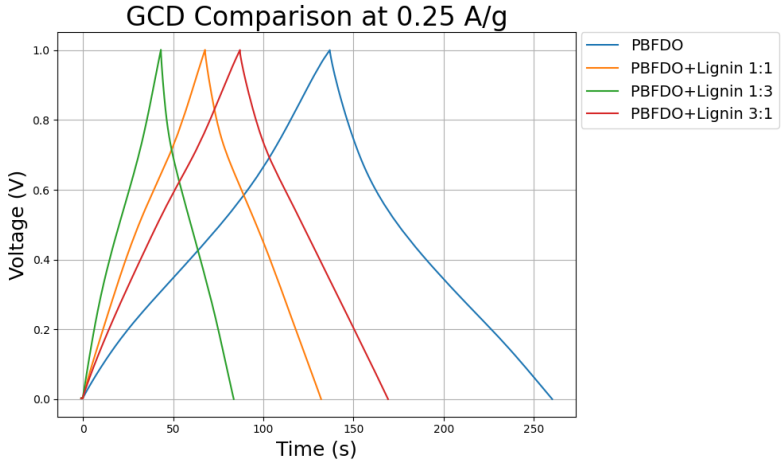

Figure 4.4: Galvanostatic charge-discharge (GCD) curves of pure PBFDO and PBFDO/lignin composites (mass ratios of 3:1, 1:1, and 1:3) evaluated at a current density of 0.25 A/g.

The GCD analyses in Figure 4.4 corroborated the CV findings. Evaluated at a comparative current density of 0.25 A/g, all PBFDO blends maintained relatively

symmetrical and triangular discharge curves, however, the discharge times sequentially shortened as the lignin concentration increased. The specific capacitance of pure PBDFO was calculated to be 158.2 F/g. This dropped to 93.0 F/g for the 3:1 composite, which declined further to 75.9 F/g for the 1:1 blend, and bottomed out at 35.1 F/g for the 1:3 blend. Although the PBFDO polymer matrix proved far more capable of accommodating the insulating lignin than the PEDOT derivatives, evidenced by the lack of catastrophic IR drops seen in the PEDOT composites, the biomass additive did not enhance overall capacitance. While cyclic voltammetry revealed some electrochemical activity via a distinct new signal at +0.6 V, lignin ultimately failed to act as a meaningful pseudocapacitive contributor within the tested potential window..

4.4 Electrochemical Impedance Spectroscopy (EIS) Analysis

To elucidate the fundamental causes of the performance degradation observed in the polymer-biomass composites, Electrochemical Impedance Spectroscopy (EIS) was performed. The data is visualized using Nyquist plots, where the high-frequency x-axis intercept represents the equivalent series resistance (ESR), the diameter of the high-frequency semicircle corresponds to the charge transfer resistance (Rct) at the electrode-electrolyte interface, and the low-frequency linear tail represents the Warburg impedance associated with ion diffusion [11, 21].
The Nyquist plot for pristine PBFDO exhibited a very small ESR (approximately 1 Ω) and a nearly non-existent high-frequency semicircle, indicating highly efficient charge transfer kinetics and excellent interfacial contact between the plasma-treated carbon paper and the electrolyte. In stark contrast, the Nyquist plots for the PBFDO-lignin composites displayed markedly larger semicircles, indicating hindered charge transfer, with approximate R_{ct} values of 1.3 Ω, 2.3 Ω, and 2.7 Ω for the 1:1, 1:3, and 3:1 ratios, respectively. Interestingly, while the charge transfer resistance increased, the introduction of lignin resulted in a slight decrease in ESR for the composites (approximately 1.0 to 1.2 Ω) compared to the pristine polymer."
For the PBFDO-lignin series, the EIS data provided a mechanistic explanation for the trend observed in the CV and GCD tests. As the proportion of lignosulfonate increased from 3:1 to 1:3, both the ESR and the charge transfer resistance (Rct) systematically increased. The water-soluble nature of the lignosulfonate likely caused slight dissolution or swelling within the aqueous perchloric acid electrolyte, which, combined with its electrically insulating polymer backbone, increased the interfacial resistance and obstructed the rapid diffusion of protons (H^+) into the highly conductive PBFDO matrix. Therefore, while PBFDO is a highly robust and conductive material for aqueous supercapacitors, this specific application highlights the limitations of utilizing unmodified lignosulfonate as a redox-active additive.

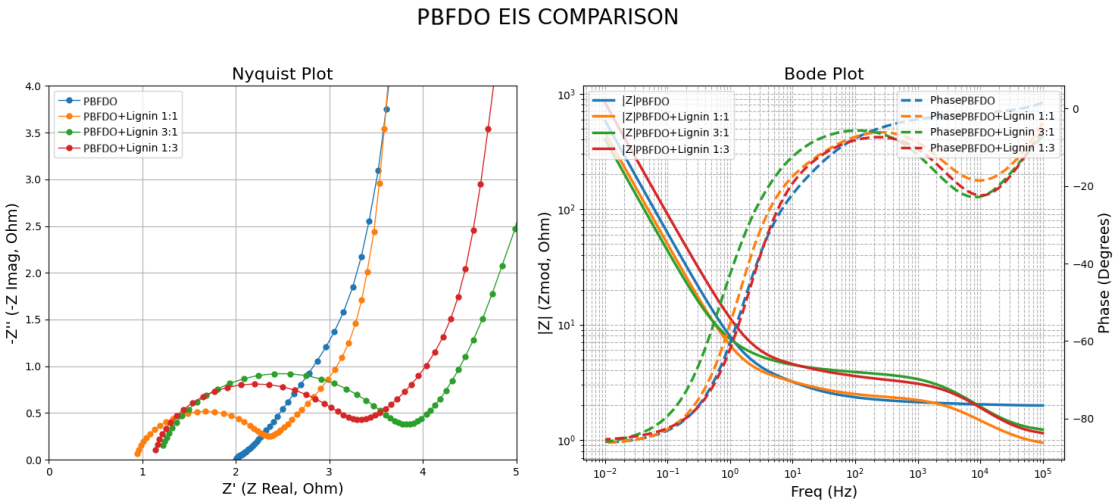

Figure 4.5: EIS comparison of PBFDO and PBFDO with lignin blends in ratios 3:1, 1:1 and 1:3.

5

Conclusion

The primary objective of this bachelor's thesis was to evaluate and compare the electrochemical performance of composites made from lignosulfonate and various conjugated polymers (the established p-type PEDOT:F and PEDOT:PSS, and the novel n-type PBFDO) as electrode materials for aqueous supercapacitors. Symmetrical two-electrode Swagelok cells with plasma-treated carbon paper substrates were successfully assembled and tested using Cyclic Voltammetry (CV), Galvanostatic Charge-Discharge (GCD), and Electrochemical Impedance Spectroscopy (EIS) to determine their practical viability [4, 11]. Based on the experimental data and comparative analysis, the following key conclusions can be drawn:

5.1 Superiority of Pristine PBFDO

In baseline testing of the pure polymers, the novel n-type PBFDO demonstrated exceptional electrochemical characteristics, vastly outperforming both PEDOT:F and PEDOT:PSS. PBFDO exhibited a highly reversible surface-mediated charge storage mechanism, minimal Equivalent Series Resistance (ESR), and high specific capacitance. This confirms recent literature highlighting PBFDO as a groundbreaking, ultra-highly conductive n-type conjugated polymer that effectively addresses the historical lack of stable n-type materials for organic energy storage [15, 18].

5.2 The Limiting Role of Lignosulfonate

The core hypothesis of this thesis was that the abundant quinone and hydroquinone substructures within lignosulfonate would undergo reversible $2e^-/2H^+$ Faradaic redox reactions, thereby providing additive pseudocapacitance when structurally confined within a conductive polymer matrix. While cyclic voltammetry did reveal a distinct new signal at +0.6 V, confirming some degree of electrochemical activity, the experimental results clearly indicate that the incorporation of unmodified lignosulfonate severely impeded the overall performance of the supercapacitor cells. Rather than acting as a synergistic redox-active contributor, the lignosulfonate effectively functioned as an electrochemically inactive, insulating dead weight. The high solubility of lignosulfonate in the aqueous perchloric acid electrolyte likely caused swelling and dissolution, which disrupted the electron transport pathways and increased the charge transfer resistance across the electrode-electrolyte interface, overwhelming any minor Faradaic benefits [2].

5.3 Comparative Resilience of PBFDO vs. PEDOT Derivatives

While the addition of lignosulfonate negatively impacted all tested polymers, the degree of degradation varied significantly. The p-type PEDOT:F and PEDOT:PSS composites suffered catastrophic performance failures at a 1:1 polymer-to-lignin mass ratio, evidenced by massive, near instantaneous IR drops and negligible discharge times. In contrast, the n-type PBFDO polymer matrix demonstrated remarkable resilience. Even though the specific capacitance of the PBFDO-lignin blends decreased systematically as the lignin concentration increased (from 3:1 to 1:1, and finally to 1:3), the PBFDO composites retained their basic quasi-rectangular CV profiles and symmetrical, triangular GCD curves without the catastrophic internal resistance spikes seen in the PEDOT cells. This suggests that the uniquely high intrinsic electrical conductivity of PBFDO (up to 5500 S/cm) allows it to accommodate and wire insulating additives far better than traditional p-type derivatives [11, 18].

5.4 Future Perspectives and Recommendations

The findings of this thesis demonstrate that while utilizing cheap, abundant biomass like lignin is an attractive route for sustainable energy storage, physical blending and drop-casting with conjugated polymers is insufficient to overcome lignin's inherent insulating nature and tendency to dissolve [2]. Future research should focus on:

1. **Chemical Cross-linking:** Instead of simple physical mixing, chemically grafting or cross-linking the lignin molecules to the conjugated polymer backbone could prevent dissolution and improve the electron transfer to the quinone groups [2, 6].
2. **Alternative Carbon Composites:** Given the outstanding baseline performance of PBFDO, future optimization of this material should explore pairing it with highly conductive, high-surface-area carbonaceous nanomaterials (such as reduced graphene oxide or carbon nanotubes) rather than raw biomass, which has been shown to yield significant synergistic improvements in energy density and cycling stability [3, 17].
3. **Utilization of Kraft Lignin:** As an alternative to lignosulfonate, future studies should investigate the use of kraft lignin, which is another major form of technical lignin obtained as a byproduct from alkaline pulping processes[2]. Preliminary internal testing has shown much better electrochemical results when using kraft lignin. Its distinct solubility profile may offer superior structural stability in aqueous acidic environments and better synergy with the highly conductive PBFDO matrix, making it a promising candidate for further composite optimization.

Ultimately, while the polymer-biomass composites did not yield the desired synergistic capacitance, this comparative analysis successfully highlights the limitations of raw lignosulfonate and rigorously establishes the novel PBFDO as a premier, highly robust n-type conjugated polymer for next-generation energy storage applications.

References

[1] O. Gerard, A. Numan, S. Krishnan, M. Khalid, R. Subramaniam, and R. Kasi, "A review on the recent advances in binder-free electrodes for electrochemical energy storage application," *Journal of Energy Storage*, vol. 50, p. 104283, 2022.

[2] X. Geng, Y. Zhang, L. Jiao, L. Yang, J. Hamel, N. Giummarella, G. Henriksson, L. Zhang, and H. Zhu, "Bioinspired ultrastable lignin cathode via graphene reconfiguration for energy storage," *ACS Sustainable Chemistry & Engineering*, vol. 5, no. 4, pp. 3553–3561, 2017.

[3] M. S. Halper and J. C. Ellenbogen, "Supercapacitors: A brief overview," *The MITRE Corporation, McLean, Virginia, USA*, vol. 1, p. 1, 2006.

[4] M. D. Stoller and R. S. Ruoff, "Best practice methods for determining an electrode material's performance for ultracapacitors," *Energy & Environmental Science*, vol. 3, no. 9, pp. 1294–1301, 2010.

[5] Y. Hu, Z. Wan, H. Song, F. Jiang, X. Liu, C. Liu, C. Liu, J. Xu, and P. Liu, "Ultralong cycle stability poly (benzodifurandione)/ti3c2tx films as novel self-supporting electrodes for supercapacitors," *Journal of Energy Storage*, vol. 135, p. 118279, 2025.

[6] K. Namsheer and C. S. Rout, "Conducting polymers: a comprehensive review on recent advances in synthesis, properties and applications," *RSC advances*, vol. 11, no. 10, pp. 5659–5697, 2021.

[7] A. V. Volkov, K. Wijeratne, E. Mitraka, U. Ail, D. Zhao, K. Tybrandt, J. W. Andreasen, M. Berggren, X. Crispin, and I. V. Zozoulenko, "Understanding the capacitance of pedot: Pss," *Advanced Functional Materials*, vol. 27, no. 28, p. 1700329, 2017.

[8] G. Liu, H.-H. Hsu, S. Samal, W.-J. Lee, Z. Ke, L. You, B. M. Savoie, and J. Mei, "Selenium dioxide catalyzed polymerization of n-doped poly (benzodifurandione)(n-pbdf) and its derivatives," *Angewandte Chemie*, vol. 137, no. 6, p. e202418668, 2025.

[9] H. Tang, Y. Liang, C. Liu, Z. Hu, Y. Deng, H. Guo, Z. Yu, A. Song, H. Zhao, D. Zhao, *et al.*, "A solution-processed n-type conducting polymer with ultrahigh conductivity," *Nature*, vol. 611, no. 7935, pp. 271–277, 2022.

[10] A. Śliwak, B. Grzyb, N. Díez, and G. Gryglewicz, "Nitrogen-doped reduced

graphene oxide as electrode material for high rate supercapacitors," *Applied Surface Science*, vol. 399, pp. 265–271, 2017.

[11] C. Liu, C. Sun, Y. Gao, W. Lan, and S. Chen, "Improving the electrochemical properties of carbon paper as cathodes for microfluidic fuel cells by the electrochemical activation in different solutions," *ACS omega*, vol. 6, no. 29, pp. 19153–19161, 2021.

[12] L. Tai, Q. Wei, J. Yang, G. Duan, C. Zhang, Y. Huang, X. Han, S. He, H. Zhao, C. Ma, *et al.*, "Plasma meets graphene: Surface engineering and functionalities," *ACS Applied Nano Materials*, vol. 8, no. 27, pp. 13584–13610, 2025.

[13] P. Stelmachowski, D. Maj, G. Grzybek, K. Kruczała, and A. Kotarba, "Functionalization of graphite with oxidative plasma," *International Journal of Molecular Sciences*, vol. 23, no. 17, p. 9650, 2022.

[14] M. Adeel, H. Lee, K. Asif, S. Smith, H. Kurt, F. Rizzolio, S. Daniele, and F. Güder, "Micro-supercapacitors for self-powered biosensors," *Small Science*, vol. 4, 05 2024.

[15] Z. Genene, Z. Xia, G. Yang, W. Mammo, and E. Wang, "Recent advances in the synthesis of conjugated polymers for supercapacitors," *Advanced Materials Technologies*, vol. 9, no. 9, p. 2300167, 2024.

[16] S. Kang, E. C. Kim, H. W. Kim, and B. Kang, "Investigation of poly (benzodifurandione) for bioelectronics: high conductivity, electrical stability, and biocompatibility," *Macromolecular Research*, vol. 33, no. 3, pp. 377–383, 2025.

[17] D. Ohayon, G. Quek, B. R. P. Yip, F. Lopez-Garcia, P. R. Ng, R. J. Vázquez, D. V. Andreeva, X. Wang, and G. C. Bazan, "High-performance aqueous supercapacitors based on a self-doped n-type conducting polymer," *Advanced Materials*, vol. 36, no. 47, p. 2410512, 2024.

[18] X. Ni, H. Li, and J.-L. Bredas, "Electronic and magnetic properties of oligomers and chains of poly (benzodifurandione)(pbdf), a highly conducting n-type polymer," *Chemistry of Materials*, vol. 35, no. 15, pp. 5886–5894, 2023.

[19] Z. Ke, A. Abtahi, J. Hwang, K. Chen, J. Chaudhary, I. Song, K. Perera, L. You, K. N. Baustert, K. R. Graham, *et al.*, "Highly conductive and solution-processable n-doped transparent organic conductor," *Journal of the American Chemical Society*, vol. 145, no. 6, pp. 3706–3715, 2023.

[20] F. Ajjan, N. Casado, T. Rębiś, A. Elfwing, N. Solin, D. Mecerreyes, and O. Inganäs, "High performance pedot/lignin biopolymer composites for electrochemical supercapacitors," *Journal of Materials Chemistry A*, vol. 4, no. 5, pp. 1838–1847, 2016.

[21] T. Guan, L. Shen, and N. Bao, "Hydrophilicity improvement of graphene fibers for high-performance flexible supercapacitor," *Industrial & Engineering Chemistry Research*, vol. 58, no. 37, pp. 17338–17345, 2019.

[22] M. Chakraborty, M. Battestini Vives, O. Y. Abdelaziz, G. Henriksson, R. Wreland Lindstrom, C. P. Hulteberg, and A. Khataee, "Lignin-based electrolytes for aqueous redox flow batteries," *ACS Sustainable Chemistry & Engineering*, vol. 12, no. 42, pp. 15409–15417, 2024.

A

Appendix

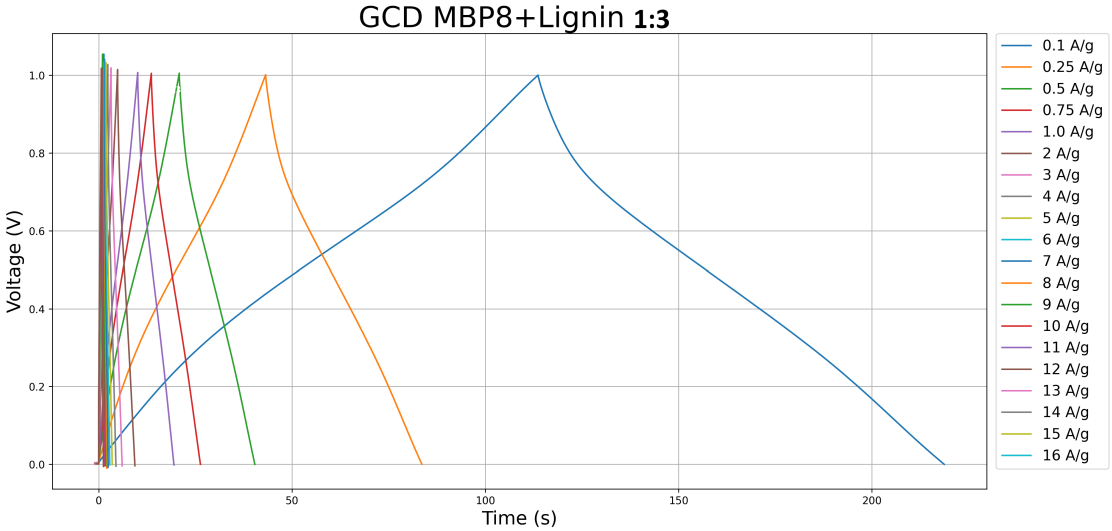

Figure A.10: GCD of PBFDO/Lignin 1:3

```
=== FINAL RESULTS ===
                      File  Cell_Capacitance_F  Specific_Capacitance_F_per_g  Discharge_R2
0   PEDOT.F_GCD_0.1Apg.DTA            0.012996                     32.490118      0.562866
1   PEDOT.F_GCD_0.5Apg.DTA            0.007771                     19.427118      0.933016
2  PEDOT.F_GCD_0.25Apg.DTA            0.013213                     33.031458      0.512541
3  PEDOT.F_GCD_0.75Apg.DTA            0.007611                     19.027478      0.933086
4   PEDOT.F_GCD_1.0Apg.DTA            0.007380                     18.450571      0.934900
5     PEDOT.F_GCD_2Apg.DTA            0.015421                     38.552050      0.458416
6     PEDOT.F_GCD_3Apg.DTA            0.005856                     14.639681      0.922232
7     PEDOT.F_GCD_4Apg.DTA            0.005448                     13.618823      0.929576
8     PEDOT.F_GCD_5Apg.DTA            0.005038                     12.595890      0.940490
```

Figure A.1: Calculated capacitance and specific capacitence for PDOT:F.

```
=== FINAL RESULTS ===
                          File  Cell_Capacitance_F  Specific_Capacitance_F_per_g  Discharge_R2
0    PEDOT.F.Lignin_GCD_0.1Apg.DTA        3.057160e-03                      0.924312      0.981785
1   PEDOT.F.Lignin_GCD_0.25Apg.DTA        2.673933e-03                      0.808445      0.987306
2    PEDOT.F.Lignin_GCD_1.0Apg.DTA        8.319263e-07                      0.000252      0.986415
3      PEDOT.F.Lignin_GCD_2Apg.DTA        3.871332e-07                      0.000117      0.987670
4      PEDOT.F.Lignin_GCD_3Apg.DTA        2.152547e-07                      0.000065      0.980673
5      PEDOT.F.Lignin_GCD_4Apg.DTA        4.222478e-06                      0.001277      0.999957
6      PEDOT.F.Lignin_GCD_5Apg.DTA        9.587807e-08                      0.000029      0.981735
7      PEDOT.F.Lignin_GCD_7Apg.DTA        6.673505e-07                      0.000202      0.982184
8      PEDOT.F.Lignin_GCD_8Apg.DTA        4.907784e-07                      0.000148      0.983967
9      PEDOT.F.Lignin_GCD_9Apg.DTA        4.606833e-07                      0.000139      0.985438
10    PEDOT.F.Lignin_GCD_10Apg.DTA        3.978245e-07                      0.000120      0.987454
11    PEDOT.F.Lignin_GCD_11Apg.DTA        3.557753e-07                      0.000108      0.990255
12    PEDOT.F.Lignin_GCD_12Apg.DTA        3.034106e-07                      0.000092      0.991911
```

Figure A.2: Calculated capacitance and specific capacitence for PDOT:F with Linosolfunate in a 1:1 ratio.

```
=== FINAL RESULTS ===
                          File  Cell_Capacitance_F  Specific_Capacitance_F_per_g  Discharge_R2
0     PEDOT.PSS_GCD_16Apg.DTA            0.000002                      0.003342      0.998844
1     PEDOT.PSS_GCD_15Apg.DTA            0.000002                      0.003587      0.998886
2     PEDOT.PSS_GCD_14Apg.DTA            0.000002                      0.003861      0.998871
3     PEDOT.PSS_GCD_13Apg.DTA            0.000003                      0.004588      0.998924
4     PEDOT.PSS_GCD_12Apg.DTA            0.000003                      0.005000      0.998952
5     PEDOT.PSS_GCD_11Apg.DTA            0.014948                     23.821109      0.998917
6     PEDOT.PSS_GCD_10Apg.DTA            0.015033                     23.956916      0.998921
7      PEDOT.PSS_GCD_9Apg.DTA            0.015118                     24.092364      0.998936
8      PEDOT.PSS_GCD_8Apg.DTA            0.015204                     24.229808      0.998953
9      PEDOT.PSS_GCD_7Apg.DTA            0.015295                     24.373836      0.998967
10     PEDOT.PSS_GCD_6Apg.DTA            0.015385                     24.517197      0.998987
11     PEDOT.PSS_GCD_5Apg.DTA            0.015483                     24.674896      0.999002
12     PEDOT.PSS_GCD_4Apg.DTA            0.015575                     24.821199      0.999019
13     PEDOT.PSS_GCD_3Apg.DTA            0.015893                     25.327387      0.998521
14   PEDOT.PSS_GCD_1.0Apg.DTA            0.018438                     29.383071      0.910088
15  PEDOT.PSS_GCD_0.75Apg.DTA            0.018211                     29.020864      0.918250
16   PEDOT.PSS_GCD_0.5Apg.DTA            0.018078                     28.809426      0.923792
17  PEDOT.PSS_GCD_0.25Apg.DTA            0.018077                     28.807921      0.926594
18   PEDOT.PSS_GCD_0.1Apg.DTA            0.018188                     28.985324      0.926974
19     PEDOT.PSS_GCD_2Apg.DTA            0.016088                     25.637955      0.998520
```

Figure A.3: Calculated capacitance and specific capacitence for PDOT:PSS.

```
=== FINAL RESULTS ===
                          File  Cell_Capacitance_F  Specific_Capacitance_F_per_g  Discharge_R2
0     PEDOT.PSS.Lignin_GCD_6Apg.DTA        0.006810                      2.058907      0.998331
1     PEDOT.PSS.Lignan_GCD_5Apg.DTA        0.006844                      2.069123      0.998409
2     PEDOT.PSS.Lignin_GCD_4Apg.DTA        0.006928                      2.094723      0.998305
3     PEDOT.PSS.Lignin_GCD_3Apg.DTA        0.007016                      2.121182      0.998151
4     PEDOT.PSS.Lignin_GCD_2Apg.DTA        0.007082                      2.141102      0.998077
5   PEDOT.PSS.Lignin_GCD_1.0Apg.DTA       17.344883                   5244.106710      0.994499
6  PEDOT.PSS.Lignin_GCD_0.25Apg.DTA        0.008425                      2.547210      0.921462
7   PEDOT.PSS.Lignin_GCD_0.1Apg.DTA       17.059711                   5157.887072      0.981336
```

Figure A.4: Calculated capacitance and specific capacitence for PDOT:PSS with Lignosolfunate in a 1:1 ratio.

=== FINAL RESULTS ===

	File	Cell_Capacitance_F	Specific_Capacitance_F_per_g	Discharge_R2
0	MBP8_GCD_0.1Apg.DTA	27.597433	111504.780949	0.999998
1	MBP8_GCD_0.25Apg.DTA	0.039160	158.222953	0.863742
2	MBP8_GCD_0.75Apg.DTA	24.982607	100939.825724	0.999998
3	MBP8_GCD_3Apg.DTA	0.028483	115.084181	0.976118
4	MBP8_GCD_4Apg.DTA	0.028191	113.902396	0.976731
5	MBP8_GCD_5Apg.DTA	0.027990	113.089318	0.976488
6	MBP8_GCD_6Apg.DTA	0.027837	112.472613	0.977245
7	MBP8_GCD_7Apg.DTA	0.027759	112.156651	0.977969
8	MBP8_GCD_8Apg.DTA	0.027555	111.335178	0.977574
9	MBP8_GCD_9Apg.DTA	0.027414	110.763126	0.977501
10	MBP8_GCD_10Apg.DTA	0.026966	108.954362	0.977407
11	MBP8_GCD_11Apg.DTA	0.026832	108.412257	0.977508
12	MBP8_GCD_12Apg.DTA	0.026699	107.875816	0.977494
13	MBP8_GCD_13Apg.DTA	0.026283	106.193930	0.976587
14	MBP8_GCD_14Apg.DTA	0.026224	105.956789	0.977185
15	MBP8_GCD_15Apg.DTA	0.026094	105.430799	0.977459
16	MBP8_GCD_16Apg.DTA	0.025931	104.772322	0.977281

Figure A.5: Calculated capacitance and specific capacitence for PBFDO

=== FINAL RESULTS ===

	File	Cell_Capacitance_F	Specific_Capacitance_F_per_g	Discharge_R2
0	1to1_MBP8_GCD_5Apg.DTA	0.037005	58.505182	0.997038
1	1to1_MBP8_GCD_6Apg.DTA	0.036761	58.120273	0.997072
2	1to1_MBP8_GCD_7Apg.DTA	0.036566	57.812099	0.996746
3	1to1_MBP8_GCD_8Apg.DTA	0.036218	57.262378	0.996771
4	1to1_MBP8_GCD_9Apg.DTA	0.036016	56.942208	0.996839
5	1to1_MBP8_GCD_10Apg.DTA	0.034664	54.804275	0.995315
6	1to1_MBP8_GCD_11Apg.DTA	0.034376	54.348811	0.995315
7	1to1_MBP8_GCD_12Apg.DTA	0.034075	53.873944	0.995050
8	1to1_MBP8_GCD_13Apg.DTA	0.045835	72.465866	0.929536
9	1to1_MBP8_GCD_14Apg.DTA	0.032587	51.521638	0.993441
10	1to1_MBP8_GCD_15Apg.DTA	0.000002	0.002502	0.982049
11	1to1_MBP8_GCD_16Apg.DTA	0.031928	50.479175	0.992703
12	1to1_MBP8_GCD_0.1Apg.DTA	39.817340	62952.316939	0.999998
13	1to1_MBP8_GCD_0.25Apg.DTA	0.048063	75.989252	0.933133
14	1to1_MBP8_GCD_1.0Apg.DTA	0.039063	61.759229	0.997241
15	1to1_MBP8_GCD_2Apg.DTA	0.038186	60.373025	0.997113
16	1to1_MBP8_GCD_3Apg.DTA	0.037666	59.550740	0.996810
17	1to1_MBP8_GCD_4Apg.DTA	0.037289	58.954226	0.996846

Figure A.6: Calculated capacitance and specific capacitence for PBFDO with Lignosolfunate in a 1:1 ratio.

```
=== FINAL RESULTS ===
                        File  Cell_Capacitance_F  Specific_Capacitance_F_per_g  Discharge_R2
0     1to3_MBP8_GCD_0.1Apg.DTA           18.500338                  32456.733963      0.999999
1    1to3_MBP8_GCD_0.75Apg.DTA            0.022015                     38.623020      0.995917
2     1to3_MBP8_GCD_1.0Apg.DTA            0.021730                     38.122546      0.995854
3       1to3_MBP8_GCD_2Apg.DTA            0.021062                     36.951232      0.995785
4       1to3_MBP8_GCD_3Apg.DTA            0.020710                     36.334034      0.996098
5       1to3_MBP8_GCD_4Apg.DTA            0.020460                     35.895106      0.996358
6       1to3_MBP8_GCD_5Apg.DTA            0.020282                     35.582300      0.995951
7       1to3_MBP8_GCD_6Apg.DTA            0.020141                     35.335310      0.996930
8       1to3_MBP8_GCD_7Apg.DTA            0.020031                     35.141332      0.995240
9       1to3_MBP8_GCD_8Apg.DTA            0.019854                     34.832109      0.995546
10      1to3_MBP8_GCD_9Apg.DTA            0.019708                     34.575241      0.995670
11     1to3_MBP8_GCD_10Apg.DTA            0.018816                     33.011349      0.994150
12     1to3_MBP8_GCD_12Apg.DTA            0.018514                     32.480781      0.993816
13     1to3_MBP8_GCD_11Apg.DTA            0.018653                     32.723713      0.993677
```

Figure A.7: Calculated capacitance and specific capacitence for PBFDO with Lignosolfunate in a 1:3 ratio.

```
=== FINAL RESULTS ===
                        File  Cell_Capacitance_F  Specific_Capacitance_F_per_g  Discharge_R2
0    3to1_MBP8_GCD_0.25Apg.DTA            0.055801                     93.001391      0.923521
1     3to1_MBP8_GCD_1.0Apg.DTA            0.045278                     75.463574      0.996877
2       3to1_MBP8_GCD_2Apg.DTA            0.043943                     73.237747      0.996701
3       3to1_MBP8_GCD_3Apg.DTA            0.043106                     71.843808      0.996635
4       3to1_MBP8_GCD_4Apg.DTA            0.042437                     70.727709      0.996207
5       3to1_MBP8_GCD_5Apg.DTA            0.041875                     69.792191      0.996475
6       3to1_MBP8_GCD_6Apg.DTA            0.041378                     68.963894      0.996394
7       3to1_MBP8_GCD_7Apg.DTA            0.040871                     68.118992      0.995989
8       3to1_MBP8_GCD_8Apg.DTA            0.040104                     66.839470      0.995510
9       3to1_MBP8_GCD_9Apg.DTA            0.039593                     65.987569      0.994722
10     3to1_MBP8_GCD_10Apg.DTA            0.037481                     62.467890      0.992207
11     3to1_MBP8_GCD_11Apg.DTA            0.036807                     61.344396      0.991591
12     3to1_MBP8_GCD_12Apg.DTA            0.036119                     60.197828      0.991430
13     3to1_MBP8_GCD_13Apg.DTA            0.034549                     57.581006      0.988563
14     3to1_MBP8_GCD_14Apg.DTA            0.033807                     56.344444      0.987599
15     3to1_MBP8_GCD_15Apg.DTA            0.033029                     55.048500      0.986403
16     3to1_MBP8_GCD_16Apg.DTA            0.032298                     53.830221      0.985028
17    3to1_MBP8_GCD_0.1Apg.DTA            0.057703                     96.171033      0.923609
```

Figure A.8: Calculated capacitance and specific capacitence for PBFDO with Lignosolfunate in a 3:1 ratio.

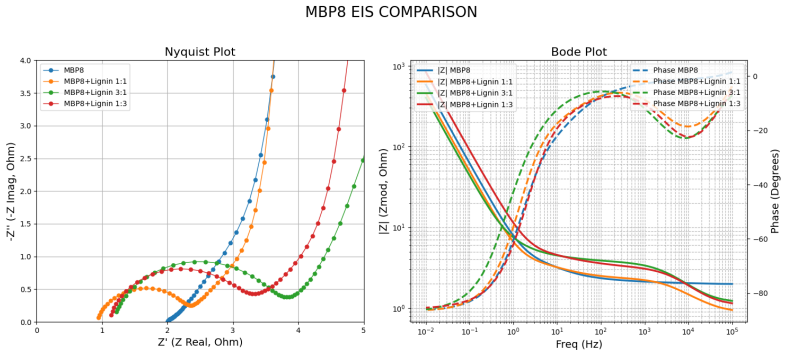

Figure A.9: EIS comparison of PBFDO and PBFDO with lignin blends in different ratios.

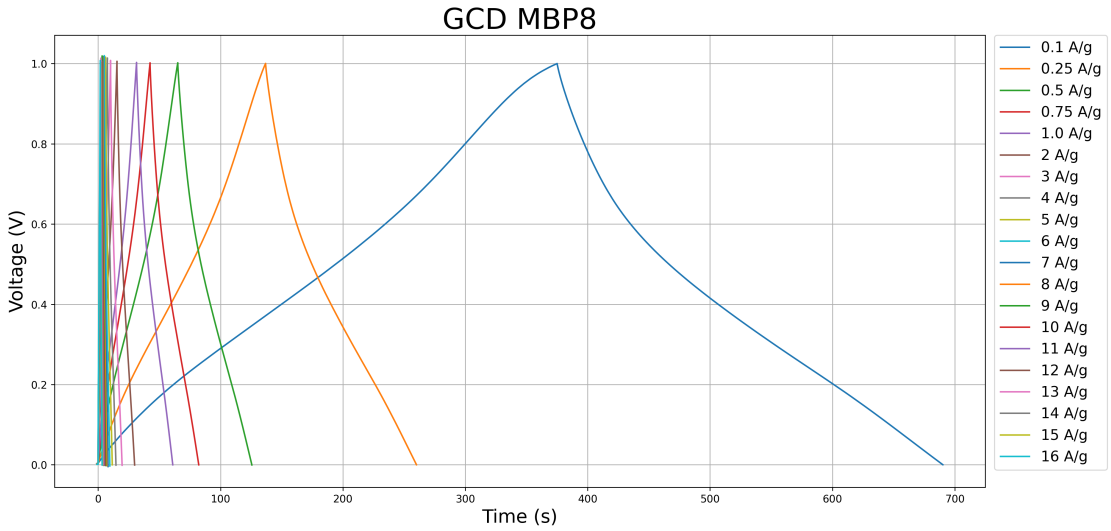

Figure A.11: GCD of PBFDO

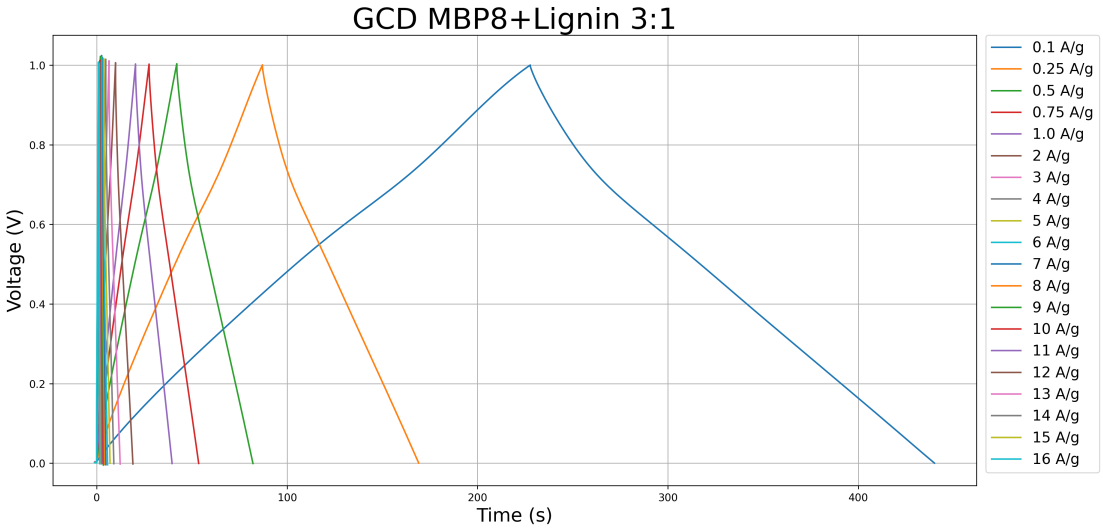

Figure A.12: GCD of PBFDO/Lignin 3:1

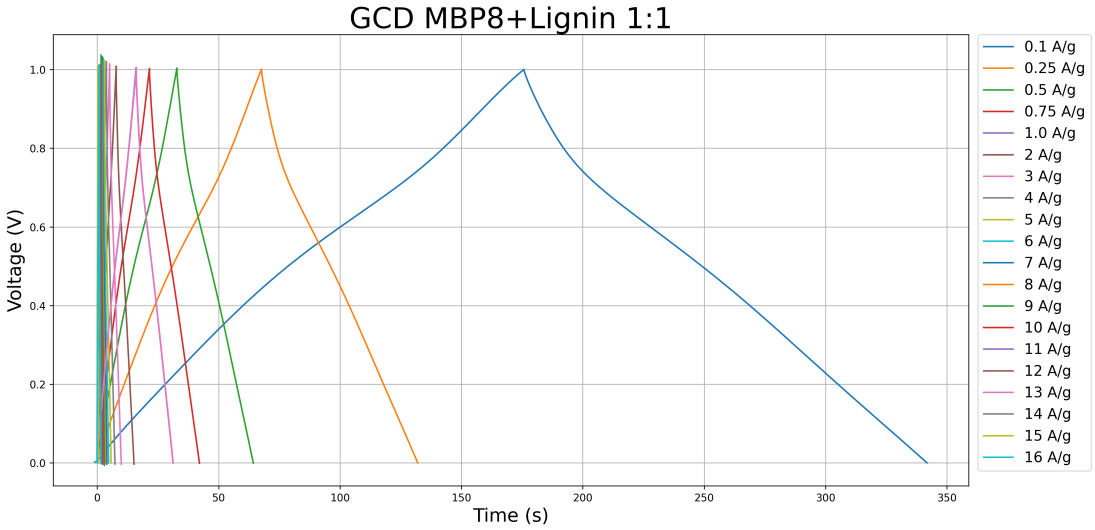

Figure A.13: GCD of PBFDO/Lignin 1:1

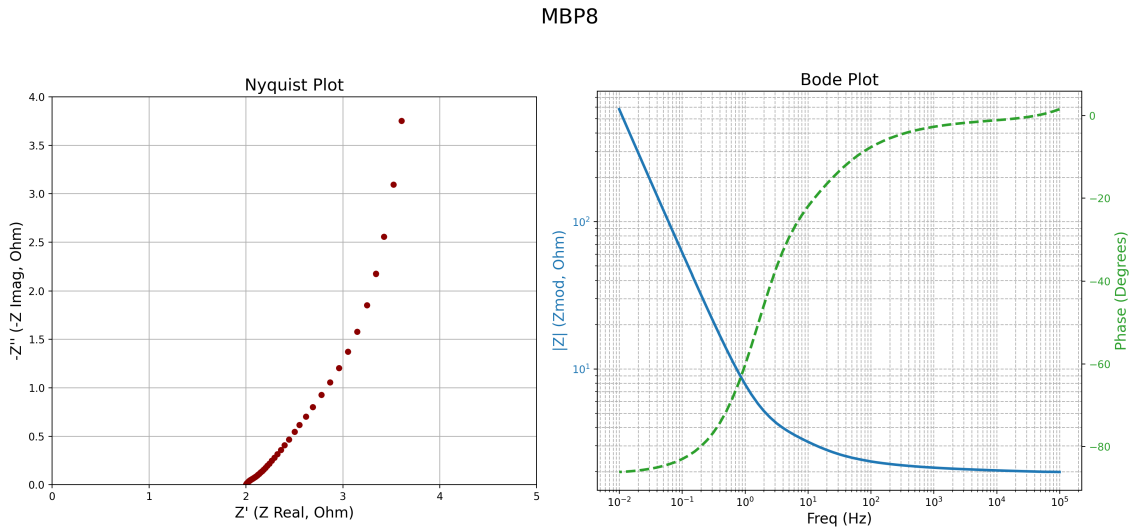

Figure A.14: EIS of PBFDO

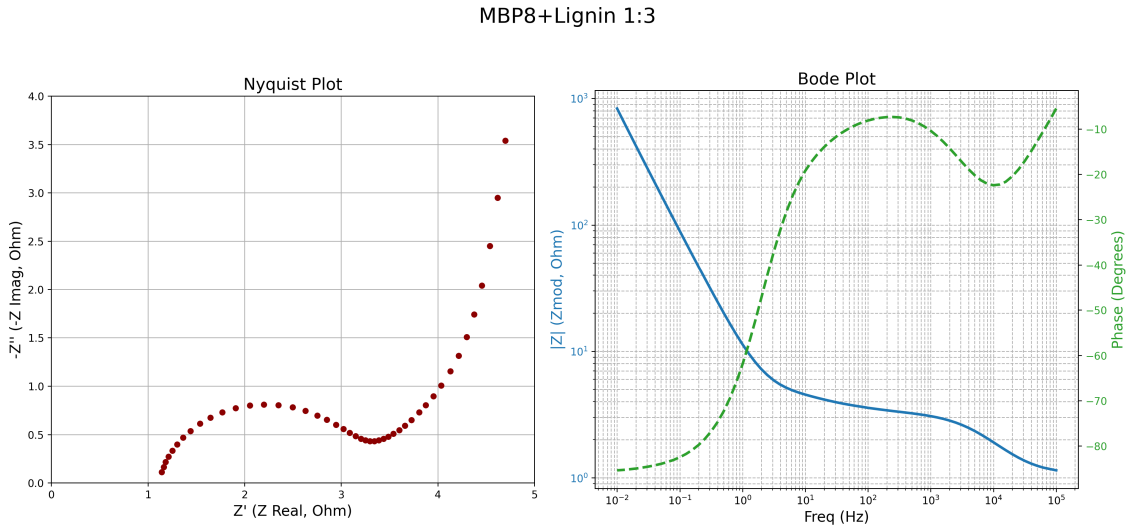

Figure A.15: EIS of PBFDO/Lignin 1:3

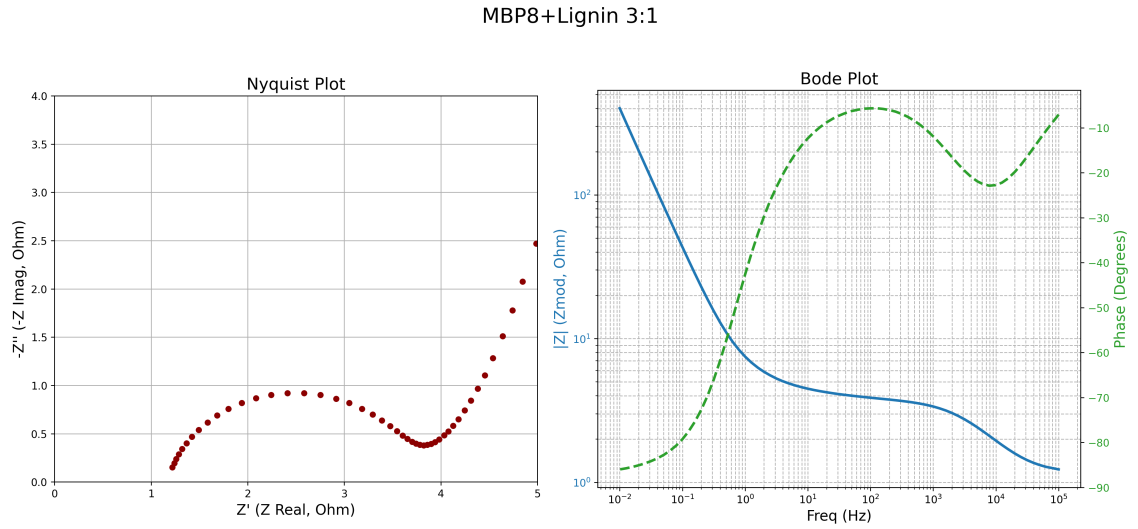

Figure A.16: EIS of PBFDO/Lignin 3:1

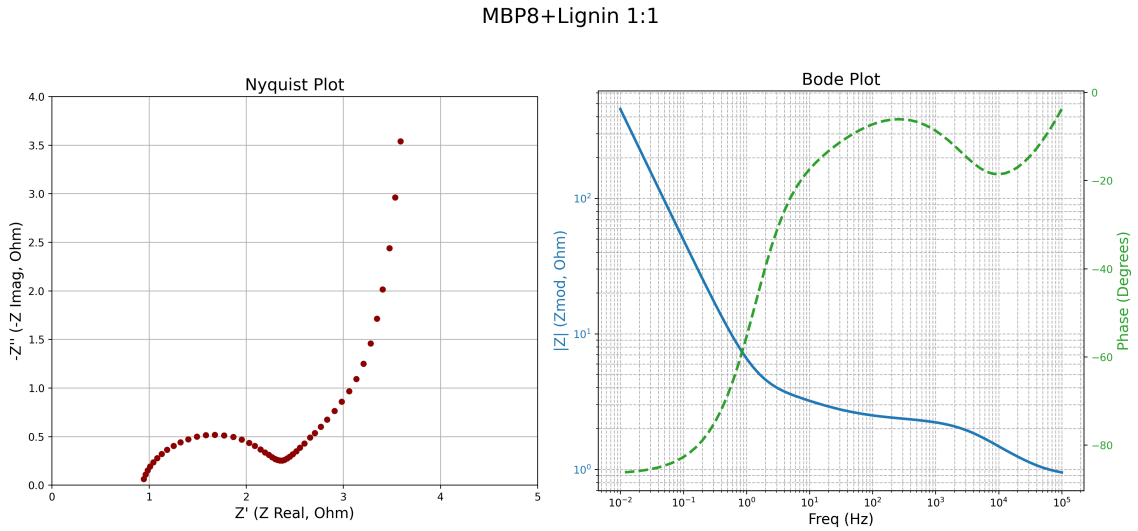

Figure A.17: EIS of PBFDO/Lignin 1:1

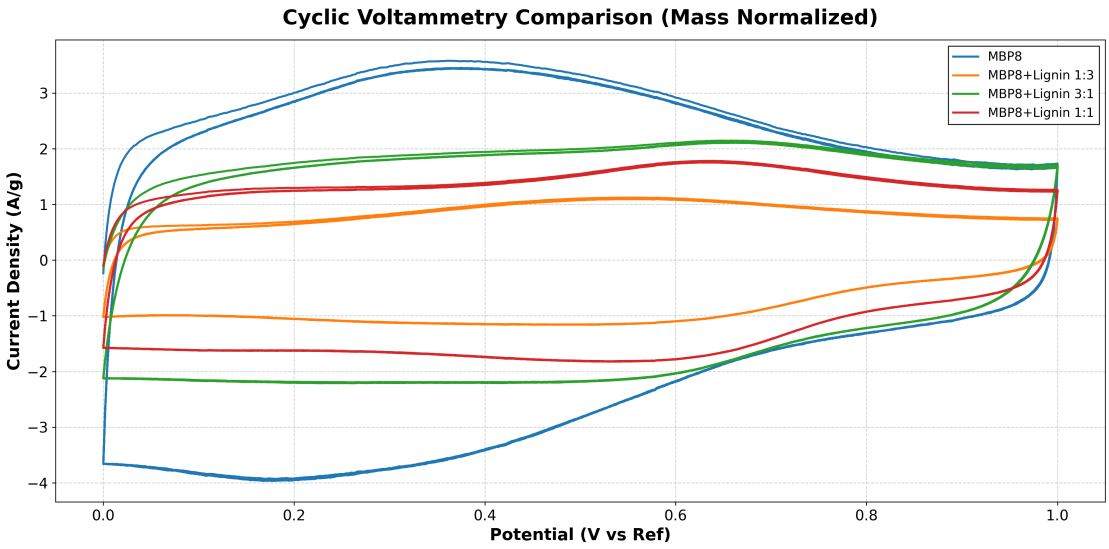

Figure A.18: CV Comparison of PBFDO and PBFDO/Lignin in 1:1,3:1 and 1:3

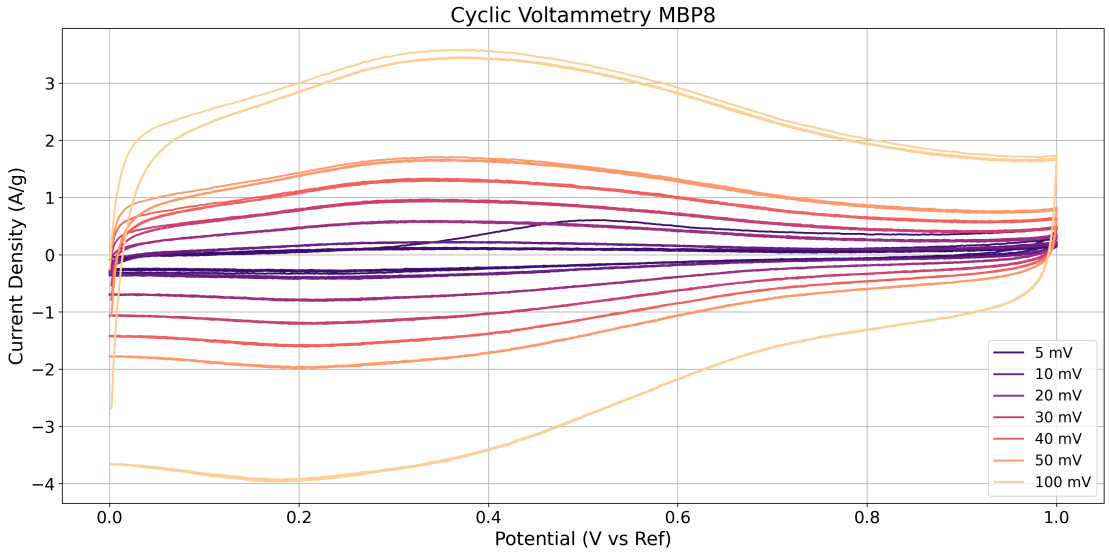

Figure A.19: CV of PBFDO

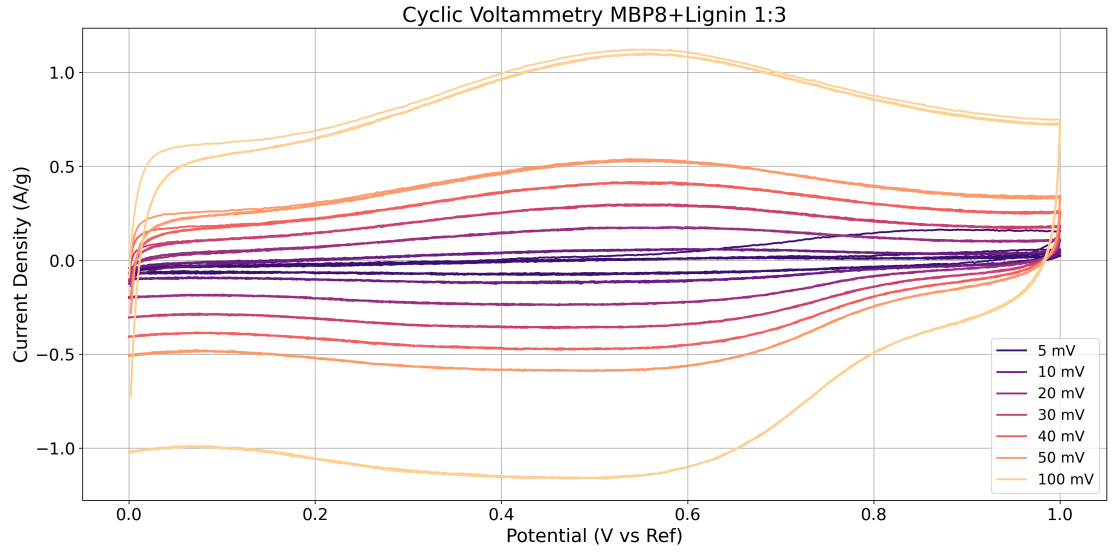

Figure A.20: CV of PBFDO/Lignin 1:3

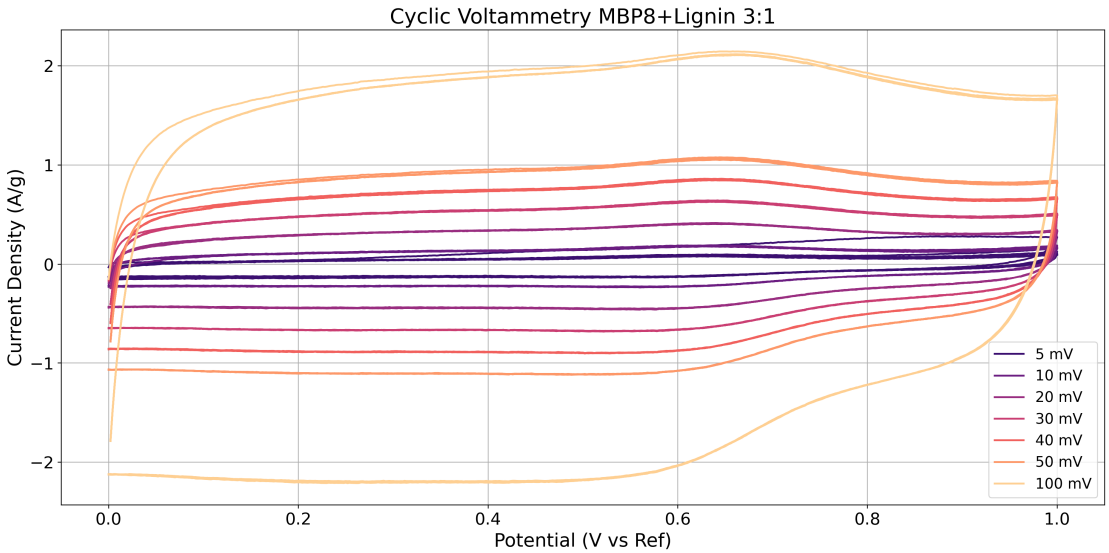

Figure A.21: CV of PBFDO/Lignin 3:1

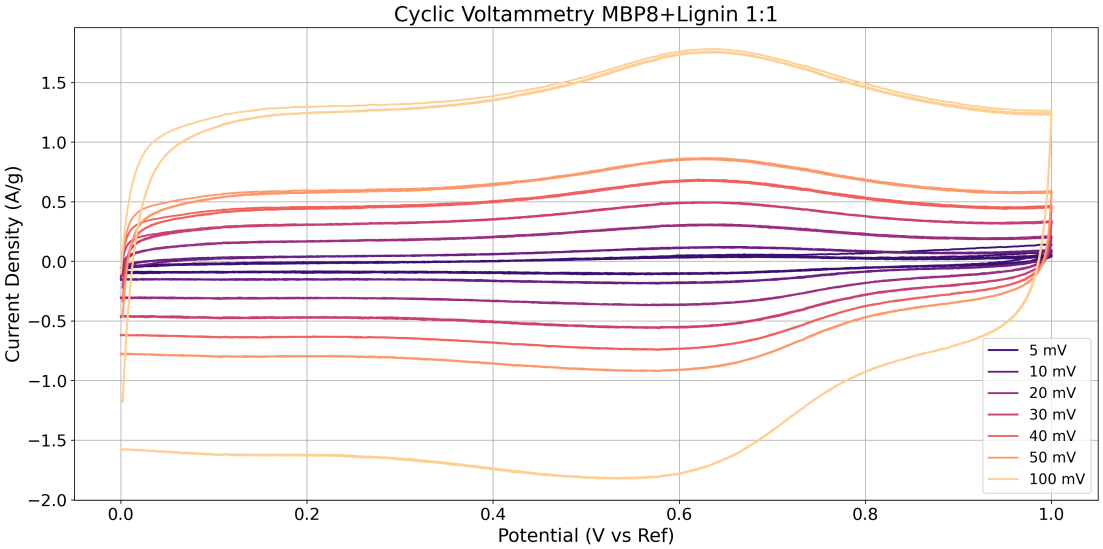

Figure A.22: CV of PBFDO/Lignin 1:1

DEPARTMENT OF SOME SUBJECT OR TECHNOLOGY
CHALMERS UNIVERSITY OF TECHNOLOGY
Gothenburg, Sweden
www.chalmers.se

CHALMERS